ISSN: 0256-307X

中国物理快报

Chinese Physics Letters

Volume 28 Number 8 August 2011

A Series Journal of the Chinese Physical Society
Distributed by IOP Publishing

Online: http://iopscience.iop.org/cpl
http://cpl.iphy.ac.cn

CHINESE PHYSICAL SOCIETY
Institute of Physics PUBLISHING

Magnetic Reconnection Under Solar Coronal Conditions with the 2.5D AMR Resistive MHD Model *

ZHANG Shao-Hua(张绍华)[1,2**], FENG Xue-Shang(冯学尚)[1], WANG Yi(王翼)[1,2], YANG Li-Ping(杨利平)[1,2]

[1]*SIGMA Weather Group, State Key Laboratory for Space Weather, Center for Space Science and Applied Research, Chinese Academy of Sciences, Beijing 100190*

[2]*College of Earth Sciences, Graduate University of Chinese Academy of Sciences, Beijing 100049*

(Received 23 March 2011)

The evolutionary process of magnetic reconnection under solar coronal conditions is investigated with our recently developed 2.5D adaptive mesh refinement (AMR) resistive magneto hydrodynamics (MHD) model. We reveal the successive fragmentation and merging of plasmoids in a long-thin current sheet with Lundquist number $R_m = 5.0 \times 10^4$. It is found that several big magnetic islands are formed eventually, with many slow-mode shocks bounding around the outflow regions. The multi-scale hierarchical-like structures of the magnetic reconnection are well resolved by the model and the AMR technique of the model can capture many fine pictures (e.g., the near-singular diffusion regions) of the development and simultaneously it can save a great deal of computing resources.

PACS: 96.60.P–, 96.60.Iv DOI:10.1088/0256-307X/28/8/089601

Magnetic reconnection is a fundamental plasma process in which magnetic field topology is rearranged and magnetic energy is converted into the kinetic and thermal energy of plasma.[1,2] It is widely accepted that magnetic reconnection plays an important role in solar flares for fast energy release and associated particle acceleration.[3–5] In the solar corona and the magnetotail, magnetic reconnection always occurs at current sheet, which is expected to form under various conditions.[6–8] Liu *et al.*[9] have recently identified a current sheet associated with many reconnection signatures, from which it is theoretically predicted that the magnetic reconnection at the current sheet is dynamic and unstable during the flare time.[10,11] A 2.5D magneto hydrodynamics (MHD) simulation carried out by Jin *et al.*[12] illustrated that the formation of plasmoids could occur intermittently and repeatedly in the course of a substorm.

In order to study the magnetic reconnection under solar coronal conditions, we solve the 2.5 D resistive MHD equations that have been described in detail by Feng *et al.*[13] However, magnetic reconnection in solar flares evolves on many scales (from 10 Mm to 10 m). The diffusion regions, where the actual breaking of magnetic field lines takes place, just occupy a small fraction of the whole computational area.[14] Thus it is difficult to study the global evolution of magnetic reconnection while at the same time to resolve the small diffusion regions when using uniform computational grids. Therefore, the adaptive mesh refinement (AMR) technique[15] is employed to deal with the multi-scale reconnection problem. The main features of the numerical algorithm and implementation of the AMR technique are briefly described as follows.

We use a splitting based finite volume scheme which splits the resistive MHD equations into a fluid part and a magnetic induction part.[16] The fluid part is solved with the second order Godunov-type central scheme[17,18] and the magnetic part is handled with constrained transport (CT) approach.[19] The second order total variation diminishing (TVD) Runge–Kutta scheme is applied for time integration. The AMR technique is achieved by utilizing an AMR package PARAMESH,[20] which provides the underlying grid and data management as well as parallel communication infrastructures. We also implement the divergence-free restriction and prolongation operators to accomplish the AMR simulation.[21] The present model has been used to study the Magnetic Cloud (MC) driven reconnection under real solar wind conditions.[22]

In this Letter, we employ the model to investigate the developing process of magnetic reconnection under solar coronal conditions,[11] not for a particular event.

The initial condition for the simulation is given by the Harris equilibrium, $B_x = B_0 \tanh(y/\lambda)$ with $\lambda = 0.5L_0$, where the magnetic field strength $B_0 = 0.004$ T and the current sheet width $L_0 = 600$ km. The guide field is given as $B_z = 0.2B_0$ and the temperature is 2.0×10^6 K. To balance the total pressure, the density is chosen to be $\rho = \rho_0 \mathrm{sech}^2(y/\lambda) + 0.2\rho_0$ with $\rho_0 = 2.1 \times 10^{-11}$ kg/m^3. The resistivity η ($\equiv {R_m}^{-1}$)

*Supported by the National Natural Science Foundation of China under Grant Nos 41031066, 40921063, 40874091, 40890162, 41074122 and 40536029, the National Basic Research Program of China under Grant No 2006CB806304, and the Specialized Research Fund for State Key Laboratories.

**shzhang@spaceweather.ac.cn

is uniform and constant, and $R_m = 5.0 \times 10^4$. The velocities are set to be zero. The characteristic Alfvén speed, time and current density are $V_0 = \mathrm{B}_0/\sqrt{\mu\rho_0} = 814\,\mathrm{km/s}$, $T_0 = L_0/V_0 = 0.74s$ and $J_0 = B_0/(\mu L_0) = 5.3 \times 10^{-3}\,\mathrm{A}$, respectively. The simulation box size is $(-38.4, 38.4)L_0 \times (-5.12, 5.12)L_0$ under open boundary conditions imposed on both x and y directions. To trigger the reconnection, a small perturbations is seeded at $(0,0)L_0$ with the same type as given by Birn *et al.*[23]

The numerical results are given in the following.

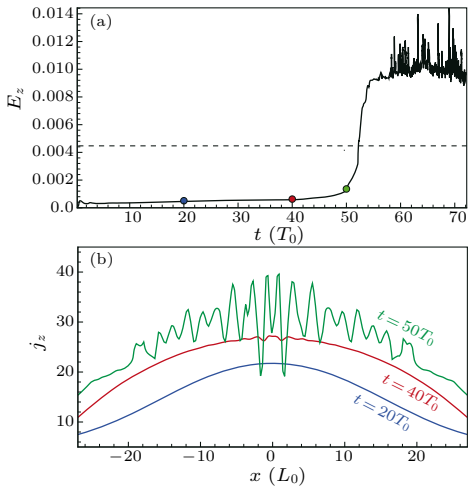

Fig. 1. (a) The profile of maximum E_z with time (solid line), in which the green point represents the onset of secondary islands; the dashed line denotes the predicted reconnection rate E_{sp} of classical SP model. (b) The variations of j_z (normalized by J_0) along x direction through the current sheet center (horizontal cut of $y = 0$) at different times.

Figure 1(a) is the temporal evolution of the maximum electric field of $E_z = \eta j_z$, where j_z denotes the out-of-plane component of the current density. E_z can be considered as the magnetic reconnection rate, although many X points appear after $t = 50T_0$. The predicted reconnection rate of the classical Sweet–Parker (SP) model is $E_{sp} = 1/\sqrt{R_m} = 0.00447$, which is plotted as the dashed line in Fig. 1(a).

Figure 1(a) exhibits that E_z rises quickly at $t = 50T_0$ (marked by the green point), the jump of which indicates the onset of secondary islands because of tearing instability.[24–26] E_z exceeds E_{sp} when secondary islands appear evidently, which can dramatically influence the reconnection rate of the system.[27–29] Figure 1(b) displays the variations of j_z along x direction through the current sheet center for different times marked by blue, red and green points in Fig. 1(a). The profile of j_z at $t = 20, 40T_0$ shows that j_z has a Gaussian-like distribution along the current sheet and it increases with time. At $t = 50T_0$, j_z has evident fluctuations, which flags the starting of the fragmentation of the current sheet.[29]

Figure 2 is the contour plots of j_z at $t = 40, 53, 57, 60, 65, 70T_0$, which reveals the evolution of magnetic islands in the reconnection process.

The magnetic reconnection triggered by the initial disturbance leads to the formation of a Sweet–Parker layer (Fig. 2(a)). In this process, the current sheet becomes thinner and longer, and j_z is enhanced. Then at about $t = 50T_0$, the secondary islands start to take place along the current sheet. They first appear evidently close to the center of the current sheet (Fig. 2(b)) and later at further away places (Fig. 2(c)). These islands become larger in size with time, moving with the reconnection outflow to the left and right sides (Fig. 2(d)). Some of the moving islands can interact and merge with each other to become larger ones (Figs. 2(e) and (f)).

After $t = 60T_0$, the reconnection process is impulsive and bursty. The continual formation and coalescence of the magnetic islands lead to the intermittent characters of E_z as demonstrated in Fig. 1(a). As the reconnection evolves, the X points between the previously formed magnetic islands can collapse into secondary current sheets,[30] which go unstable again due to tearing instability (Fig. 2(e)). As a result, smaller magnetic islands are formed, which catch up with the islands generated before and coalesce with them. Eventually, a multi-scale hierarchical-like structure is produced (Fig. 2(f)), which is similar to the concept of fractal reconnection.[31]

Figure 2(g) displays the enlarged view of a selected box in Fig. 2(f). Locally, the reconnection can be described as a Petschek-like model, with a pair of slow-mode shocks bounding around the outflow region where j_z is notably enhanced (Fig. 2(g)). The profile of the cut through y direction at $x = 10.8L_0$ shows clearly that a pair of slow-mode shocks (S1 and S2) is formed (Fig. 2(h)), which are characterized by the increase in plasma density ρ and velocity $|\boldsymbol{V}|$ and the decrease in magnetic field strength $|\boldsymbol{B}|$ (along $+y$ and $-y$ directions for S1 and S2, respectively).

The slow-mode shocks can accelerate the plasma to super-Alfvénic flows. As shown in Figs. 2(e), 2(f) and 2(g), the piston effect of these super-Alfvénic flows makes the formation of turbulent-like compression structures on the two sides of the large magnetic islands. Through the slow shocks, magnetic energy can be effectively converted into the kinetic and thermal energy of plasma by motor effect as measured by $C_{\mathrm{motor}} = \boldsymbol{V} \cdot (\boldsymbol{J} \times \boldsymbol{B})$.[3] Figure 2(h) exhibits that C_{motor} increases rapidly around the slow-mode shocks, which means that the magnetic energy conversion is fast. The process of this energy conversion may be responsible for explosive release of magnetic energy in solar flare phenomena.[3,32]

From the above results, we can see that the multi-scale structures are well resolved by our model. This is

owing to the fact that in the developing process of the magnetic reconnection, our model adjusts the computational grids automatically and dynamically to capture the refined pictures. In order to validate this, we present the j_z contour plot overlaid with AMR blocks at $t = 65T_0$ (Fig. 3(a)) and its enlarged views of some selected regions (Figs. 3(b), 3(c), 3(d) and 3(e)).

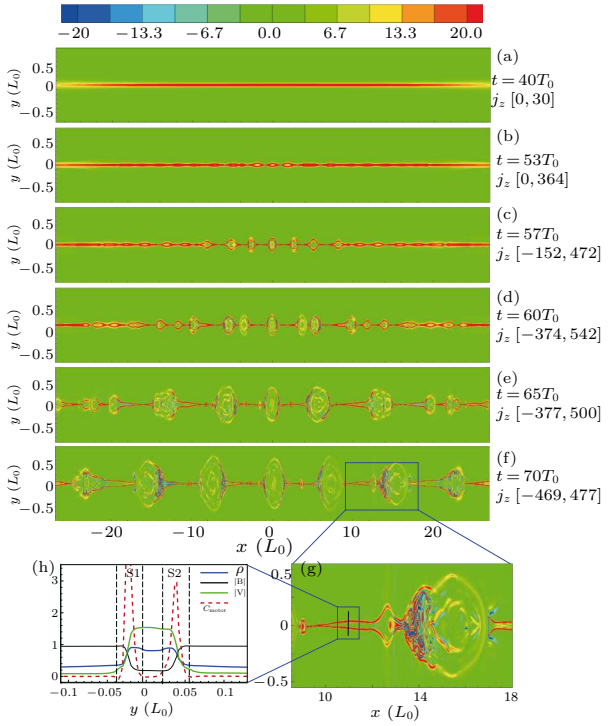

Fig. 2. (a)–(f) The j_z contour plots, which reveal the development of magnetic islands. Here j_z is normalized by J_0. It should be noted that for better visualization, the x/y axis ratio is set to 0.5 and only the central part of the numerical region is shown. (g) Enlarged view of the selected box in (f). (h) The profiles of ρ, $|\boldsymbol{B}|$, $|\boldsymbol{V}|$ and C_{motor} at cut of $x = 10.8\ L_0$, in which the values are normalized by ρ_0, B_0, V_0 and $V_0 J_0 B_0$, respectively, and the vertical long dashed lines bracket a pair of slow shocks (S1 and S2).

In Fig. 3(a) there are 16000 blocks with refinement levels of 2–8 and each one has 12×6 grids. The AMR blocks are adapted with the magnetic islands and current sheets, which are different in scales and shapes. We are able to achieve a minimum grid spacing of $\Delta x = 2.08 \times 10^{-3} L_0$ and $\Delta y = 8.33 \times 10^{-4} L_0$ in x and y directions, respectively, with only about 1.14×10^6 grid points. However, it needs about 4.53×10^8 grid points to obtain the same grid resolution when we use uniform computational grids.

It can be seen from Figs. 3(a), 3(b) and 3(d) that the width of the generated magnetic islands spans from about $1.0L_0$ to $0.06L_0$. The generation of islands can make the current sheet become thinner, as noted previously by Shibata *et al.*[31] and Loureiro *et al.*[30] If the thinner current sheet is not resolved by enough grids, excessive numerical dissipation can be introduced, which could degrade the results. Thanks to the AMR ability of the model, new computational blocks are automatically added to the dynamically evolved current sheets to make sure that the current sheets are always well resolved. Figure 3(e) is a cut of j_z in y direction at $x = 2.8L_0$ where the thinnest current sheet locates. There are 12 grid points across the current sheet, confirming that the grid resolution is sufficient for the diffusion region.

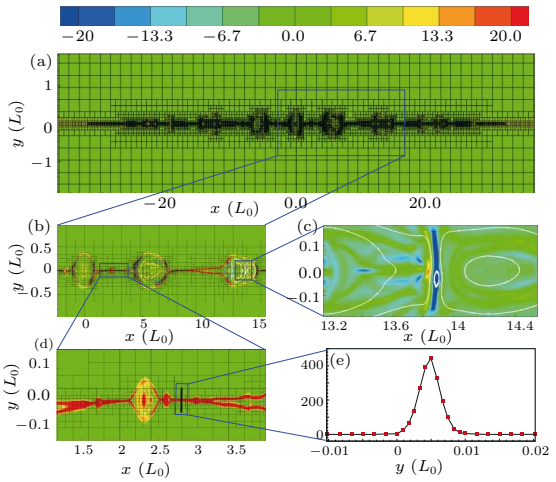

Fig. 3. (a) The j_z contour plot overlaid with AMR blocks of different refinement levels at $t = 65T_0$ and its enlarged views (b), (c) and (d). The white lines in (b) and (c) denote the magnetic filed lines. (e) Cut of j_z in y direction at $x = 2.8L_0$ where the thinnest current sheet locates, and the red square symbols are grid points.

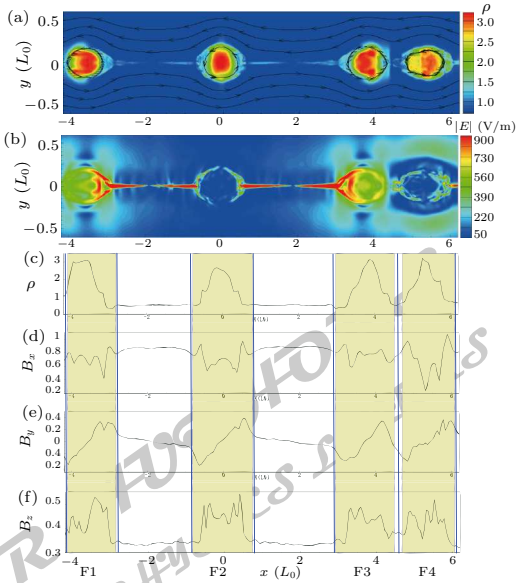

Fig. 4. (a) The contour plot of ρ overlapped with magnetic lines. (b) The contour plot of reconnection electric field $|\boldsymbol{E}|$. (c)–(f) The profiles of ρ, B_x, B_y and B_z along x direction at $y = -0.1L_0$, in which the shade areas are four flux rope structures. The values of ρ and magnetic field are normalized by ρ_0 and B_0.

Zooming into the interaction region of two large merging magnetic islands (Fig. 3(c)), we observe that

a anti-direction current sheet (perpendicular to the original horizontal current sheet) is formed between the two islands, where tearing instability also takes place. A very small island appears at $(13.9, -0.05)L_0$, which is correctly caught by the AMR blocks. If the grid resolution is insufficient, this fine structure will be dissipated.[14] Oka *et al.*[33] found that the anti-direction reconnection plays an important role in accelerating electrons by using particle-in-cell (PIC) simulation.

With the dynamic evolution of the reconnection, the reconnection electric field $\boldsymbol{E} = -\boldsymbol{V}\times\boldsymbol{B}+\eta\boldsymbol{J}$ is also developed drastically. For example, at $t = 60T_0$ when a chain of magnetic islands has been formed obviously (Fig. 4(a)), $|\boldsymbol{E}|$ can be as strong as a few hundreds of V/m (Fig. 4(b)), which is theoretically able to accelerate electrons up to relativistic energy as long as the acceleration status can be maintained.[4] As shown in the shade areas in Figs. 4(c), 4(d), 4(e) and 4(f), each magnetic island is associated with enhanced density ρ, W-like B_x, rotational (bi-polar) B_y and increased B_z. Thus they are multiple flux ropes,[34] which could trap the electron effectively for acceleration.[4,5] The test particle method[5] under these time-varying electric and magnetic fields may be helpful to further understand the acceleration process of electrons.

In conclusion, on the basis of a 2.5D resistivity MHD simulation, we have studied the dynamic and burst processes of magnetic reconnection under solar coronal conditions. The results show that the initially formed, extended Sweet–Parker-like current layer is broken up into several large magnetic islands with smaller islands continually being produced and merged with them. The outflow regions between the islands are bounded with slow-mode shocks, by which magnetic energy can be effectively converted into plasma energies. This simulated reconnection scenario can be seen as a possible process of fast magnetic energy release and effective particle acceleration, which can occur in current sheets involved in solar flares and in the interaction region between two flux ropes.[9,29,26] Moreover, taking advantages of the AMR technique, the model can automatically resolve many fine structures, e.g., near-singular diffusion regions and very small islands formed between two merging islands, and at the same time can significantly save computational resources, which is especially favorable for our further three-dimensional magnetic reconnection studies of solar flares.

The simulations were completed on our SIGMA Cluster computing system.

References

[1] Aschwanden M J 2002 *Space Sci. Rev.* **101** L1
[2] Birn J and Priest E R 2006 *Enlarge Image Reconnection of Magnetic Fields: Magnetohydrodynamics and Collisionless Theory and Observations* (Cambridge: Cambridge University)
[3] Ugai M 2001 *Space Sci. Rev.* **95** L601
[4] Litvinenko Y E 2000 *Solar Phys.* **194** L327
[5] Gordovskyy M, Browning P K and Vekstein G E 2010 *Astrophys. J.* **720** L1603
[6] Kopp R A and Pneuman G W 1976 *Solar Phys.* **50** L85
[7] Karpen J T, Antiochos S K and Devore C R 1995 *Astrophys. J.* **450** L422
[8] Priest E R and Forbes T G 2002 *Astron. Astrophys. Rev.* **10** L313
[9] Liu R et al 2010 *Astrophys. J. Lett.* **723** L28
[10] Kliem B, Karlický M and Benz A O 2000 *Astron. Astrophys.* **360** L715
[11] B árta M, Karlický M and Zemlicka R 2008 *Solar Phys.* **253** L173
[12] Jin S P et al 2001 *J. Geophys. Res.* **106** L29807
[13] Feng X S, Hu Y Q and Wei F S 2006 *Solar Phys.* **235** L235
[14] B árta M, B üchner J and Karlický M 2010 *Adv. Space Res.* **45** L10
[15] Berger M J and Oliger J 1984 *J. Comput. Phys.* **53** L484
[16] Fuchs F G, Mishra S and Risebro N H 2009 *J. Comput. Phys.* **228** L641
[17] Kurganov A, Noelle S and Petrova G 2001 *SIAM J. Sci. Comput.* **23** L707
[18] Ziegler U 2004 *J. Comput. Phys.* **196** L393
[19] T óth G 2000 *J. Comput. Phys.* **161** L605
[20] MacNeice et al 2000 *Comput. Phys. Commun.* **126** L330
[21] Li S T and Li H 2004 *J. Comput. Phys.* **199** L1
[22] Wang Y et al 2010 *Phys. Rev. Lett.* **105** L195007
[23] Birn J et al 2001 *J. Geophys. Res.* **106** L3715
[24] Loureiro N F, Schekochihin A A and Cowley S C 2007 *Phys. Plasmas* **14** L100703
[25] Samtaney R et al 2009 *Phys. Rev. Lett.* **103** L105004
[26] Huang Y M and Bhattacharjee A 2010 *Phys. Plasmas* **17** L062104
[27] Cassak P A, Shay M A and Drake J F 2009 *Phys. Plasmas* **16** L120702
[28] Wang R S et al 2010 *Phys. Rev. Lett.* **104** L175003
[29] Cassak P A and Shay M A 2011 *Space Sci. Rev.* **011** L1
[30] Loureiro N F et al 2005 *Phys. Rev. Lett.* **95** L235003
[31] Shibata K and Tanuma S 2001 *Earth, Planets, and Space* **53** L473
[32] Tsuneta S 1996 *Astrophys. J.* **456** L840
[33] Oka M et al 2010 *Astrophys. J.* **714** L915
[34] Zong Q G et al 2004 *Geophys. Res. Lett.* **31** L18803

Chinese Physics Letters

Volume 28 Number 8 August 2011

GENERAL

080201 Solving Method for the Single-Kink Soliton Solution to a Disturbed Coupled Burgers System
YAO Jing-Su, CHEN Li-Hua, WEN Zhao-Hui, MO Jia-Qi

080301 Geometric Phase for a Qutrit-Qubit Mixed-Spin System
ZHANG Ai-Ping, QIANG Wen-Chao, LING Ya-Wen, XIN Hong, YANG Yong-Ming

080302 Implementation of Quantum Private Queries Using Nuclear Magnetic Resonance
WANG Chuan, HAO Liang, ZHAO Lian-Jie

080303 N-Qubit W State of Spatially Separated Atoms via Fractional Adiabatic Passage
ZHENG An-Shou, LIU Ji-Bing, CHEN Hong-Yun

080401 Feasibility for Testing the Equivalence Principle with Optical Readout in Space
GAO Fen, ZHOU Ze-Bing, LUO Jun

080501 Pseudo-Random Sequences Generated by a Class of One-Dimensional Smooth Map
WANG Xing-Yuan, QIN Xue, XIE Yi-Xin

080502 Size Model of Critical Temperature for Grain Growth in Nano V and Au
LU Yun-Bin, LIAO Shu-Zhi, PENG Hao-Jun, ZHANG Chun, ZHOU Hui-Ying, XIE Hao-Wen, OUYANG Yi-Fang, ZHANG Bang-Wei

080601 Feasibility of Extreme Ultraviolet Active Optical Clock
ZHUANG Wei, CHEN Jing-Biao

080701 Micropore Structure Representation of Sandstone in Petroleum Reservoirs Using an Atomic Force Microscope
BAI Yong-Qiang, ZHU Xing, WU Jun-Zheng, BAI Wen-Guang

080702 Room-Temperature NH_3 Gas Sensor Based on Hydrothermally Grown ZnO Nanorods
WEI Ang, WANG Zhao, PAN Liu-Hua, LI Wei-Wei, XIONG Li, DONG Xiao-Chen, HUANG Wei

THE PHYSICS OF ELEMENTARY PARTICLES AND FIELDS

081201 Analysis of Mass Difference of the π and ρ with Bethe–Salpeter Equation
WANG Zhi-Gang

081202 Lattice QCD Study of the σ Meson
FU Zi-Wen

081301 Large Dimuon Asymmetry and a Non-Universal Z' Boson in the $B_s - \bar{B}_s$ System
CHANG Qin, WANG Ru-Min, XU Yuan-Guo, CUI Xiao-Wei

081401 Effect of Excited and Fourth Generation Leptons in Lepton Flavor Violating $\mu^- \to e^- 2\gamma$ Decay
S. C. İnan

NUCLEAR PHYSICS

082501 Singly and Doubly Charged Projectile Fragments in Nucleus-Emulsion Collisions at Dubna Energy in the Framework of the Multi-Source Model
WANG Er-Qin, LIU Fu-Hu, Magda A. Rahim, S. Fakhraddin, SUN Jian-Xin

082502 Comparison of Fission Induced by Protons and Pions
Zafar Yasin, M. Ikram Shahzad

082801 Measurement of Cross Sections for the $^{10}B(n,\alpha)^7Li$ Reaction at 4.0 and 5.0 MeV Using an Asymmetrical Twin Gridded Ionization Chamber
ZHANG Guo-Hui, LIU Xiang, LIU Jia-Ming, XUE Zhi-Hua, WU Hao, CHEN Jin-Xiang

082901 Effects of Electron Flow Current Density on Flow Impedance of Magnetically Insulated Transmission Lines
HE Yong, ZOU Wen-Kang, SONG Sheng-Yi

ATOMIC AND MOLECULAR PHYSICS

083101 Quasi-Classical Trajectory Calculations of Reaction Stereodynamics of $H+OH(v=0,\ j=0)\rightarrow H_2+O(^3P)$
ZHAO Li, SUN Ping, LIU Chao-Zhuo

083102 Product Rotational Polarization in the $Li+HF(v=0,\ j=0)$ Reaction and Its Isotopic Variants
CHENG Jie, YUE Xian-Fang

083201 Intensity and Polarization Effects in Short-Pulse Multiphoton Ionization of Xenon
KANG Hui-Peng, WANG Chuan-Liang, LIN Zhi-Yang, CHEN Yong-Ju, WU Ming-Yan, QUAN Wei, LIU Hong-Ping, LIU Xiao-Jun

083202 Relative Phase Dependence of Double Ionization in a Synthesized Laser Pulse
WANG Yuan-Sheng, XIA Chang-Long, GUO Jing, LIU Xue-Shen

083203 Radiation-Induced Nano-Explosions at the Solid Surface: Near Surface Radiation Damage in CR-39 Polymer
Mukhtar Ahmed Rana

083301 Investigation of Linear Tetra-Atomic Negative Ion by Photodetached-Electron Spectra
A. Rahman, Iftikhar Ahmad, A. Afaq, M. Haneef, H. J. Zhao

083401 Two-Fermion Scattering on Momentum-Representation in a Trap and Their Periodic Phenomena
FANG Yi-Zhong, HE Yan-Zhang

083701 Photoassociative Production and Detection of Ultracold Polar RbCs Molecules
JI Zhong-Hua, ZHANG Hong-Shan, WU Ji-Zhou, YUAN Jin-Peng, ZHAO Yan-Ting, MA Jie, WANG Li-Rong , XIAO Lian-Tuan, JIA Suo-Tang

FUNDAMENTAL AREAS OF PHENOMENOLOGY(INCLUDING APPLICATIONS)

084101 Proton Acceleration with Double-Layer Targets in the Radiation Pressure Dominant Regime
XIA Chang-Quan, DENG Ai-Hua, LIU Li, WANG Wen-Tao, LU Hai-Yang, WANG Cheng, LIU Jian-Sheng

084201 Design of a Novel Polarized Beam Splitter Based on a Two-Dimensional Photonic Crystal Resonator Cavity
ZHANG Xuan, CHEN Shu-Wen, LIAO Qing-Hua, YU Tian-Bao, LIU Nian-Hua, HUANG Yong-Zhen

084202 Single Mode Condition and Power Fraction of Air-Cladding Total Refractive Guided Porous Polymer Terahertz Fibers
JING Lei, YAO Jian-Quan

084203 Optical Noise Analysis in Dual-Resonator Structural Micro-Optic Gyro
YU Huai-Yong, ZHANG Chun-Xi, FENG Li-Shuang, HONG Ling-Fei, WANG Jun-Jie

084204 Diode-Pumped Soliton and Non-Soliton Mode-Locked Yb:GYSO Lasers
HE Jin-Ping, LIANG Xiao-Yan, LI Jin-Feng, ZHENG Li-He, SU Liang-Bi, XU Jun

084205 Optical Properties of BDK-Doped Highly Photosensitive Sol-Gel Hybrid Film
XU Ming, SHEN Wei-Dong, ZHANG Yue-Guang, ZHEN Hong-Yu, LIU Xu

084206 Large-Mode-Area Double-Cladding Photonic Crystal Fiber Laser in the Watt Range at 980 nm
LI Ping-Xue, ZHANG Xue-Xia, LIU Zhi, CHI Jun-Jie

084207 A High Power Single Frequency Diode Side-Pumped Nd:YAG Ring Laser
XIE Shi-Yong, BO Yong, XU Jia-Lin, WANG Zhi-Chao, PENG Qin-Jun, CUI Da-Fu, XU Zu-Yan

084208 Third-Order Optical Nonlinearities of Squarylium Dyes with Benzothiazole Donor Groups Measured Using the Picosecond Z-Scan Technique
LI Zhong-Yu, XU Song, CHEN Zi-Hui, ZHANG Fu-Shi, KASATANI Kazuo

084209 Reduction of the Far-Field Divergence Angle of an 850 nm Multi-Leaf Holey Vertical Cavity Surface Emitting Laser
ZHOU Kang, XU Chen, XIE Yi-Yang, ZHAO Zhen-Bo, LIU Fa, SHEN Guang-Di

084210 Light Scattering of Rough Orthogonal Anisotropic Surfaces with Secondary Most Probable Slope Distributions
LI Hai-Xia, CHENG Chuan-Fu

084211 Experimental Observation of Near-Field Deterioration Induced by Stimulated Rotational Raman Scattering in Long Air Paths
WANG Jing, ZHANG Xiao-Min, HAN Wei, LI Fu-Quan, ZHOU Li-Dan, FENG Bin, XIANG Yong

084212 Compact 2×2 Multi-Mode Interference Couplers with Uneven Splitting-Ratios Based on Silicon Nanowires
ZHOU Jing-Tao, SHEN Hua-Jun, YANG Cheng-Yue, LIU Huan-Ming, TANG Yi-Dan, LIU Xin-Yu

084213 Measurement of Temperature Change in Nonlinear Optical Materials by Using the *Z*-Scan Technique
DONG Shu-Guang, YANG Jun-Yi, SHUI Min, YI Chuan-Xiang, LI Zhong-Guo, SONG Ying-Lin

084214 A Digital Phase Lock Loop for an External Cavity Diode Laser
WANG Xiao-Long, TAO Tian-Jiong, CHENG Bing, WU Bin, XU Yun-Fei, WANG Zhao-Ying, LIN Qiang

084301 Nondestructive Characterization of Quantitative Bonding Strength at a Bonded Solid-Solid Interface
CHEN Jian-Jun, ZHANG De, MAO Yi-Wei, CHENG Jian-Chun

084302 Simultaneous Measurements of Harmonic Waves at Fatigue-Cracked Interfaces
Hyunjo Jeong, Dan Barnard

084701 MHD Flow of an Oldroyd-B Fluid through a Porous Space Induced by Sawtooth Pulses
Masood Khan, Zeeshan

084702 Dual Solutions in Unsteady Stagnation-Point Flow over a Shrinking Sheet
Krishnendu Bhattacharyya

084703 Experimental Investigation of Flow Drag and Turbulence Intensity of a Channel Flow with Rough Walls
ZHANG Hui-Qiang, LU Hao, WANG Bing, WANG Xi-Lin

084704 Instability Criterion of One-Dimensional Detonation Wave with Three-Step Chain Branching Reaction Model
TENG Hong-Hui, JIANG Zong-Lin

084705 MHD Boundary Layer Flow of Dilatant Fluid in a Divergent Channel with Suction or Blowing
Krishnendu Bhattacharyya, G. C. Layek

084706 A Low Voltage Driven Digital-Droplet-Transporting-Chip by Electrostatic Force
GAO An-Ran, LIU Xiang, GAO Xiu-Li, LI Tie, GAO Hua-Min, ZHOU Ping, WANG Yue-Lin

084707 Peristaltic Motion of Power-Law Fluid with Heat and Mass Transfer
T. Hayat, S. Hina, Awatif A. Hendi

084708 Direct Numerical Simulation of Particle Migration in a Simple Shear Flow
LV Hong, TANG Sheng-Li, ZHOU Wen-Ping

PHYSICS OF GASES, PLASMAS, AND ELECTRIC DISCHARGES

085201 Preliminary Investigation of a Dielectric Barrier Discharge Lamp in Open Air at Atmospheric Pressure
LIU Feng, WANG Wei-Wei, CHANG Xi-Jiang, LIANG Rong-Qing

085202 Shock-Timing Experiment Using a Two-Step Radiation Pulse with a Polystyrene Target
WANG Feng, PENG Xiao-Shi, JIAO Chun-Ye, LIU Shen-Ye, JIANG Xiao-Hua, DING Yong-Kun

085203 Magnetic Fluid Flows in Porous Media
LI Ming-Jun, CHEN Liang

CONDENSED MATTER: STRUCTURE, MECHANICAL AND THERMAL PROPERTIES

086101 Mechanical Property Evaluation of GaAs Crystal for Solar Cells
JIN Min, FANG Yong-Zheng, SHEN Hui, JIANG Guo-Jian, WANG Zhan-Yong, XU Jia-Yue

086102 Effect of Iodine Additive on Thermostability of Bulk Amorphous Sulfur Prepared by Rapid Compression
LIN Sheng-Xiong, LIU Xiu-Ru, SHAO Chun-Guang, SHEN Ru, HONG Shi-Ming

086103 Hole Mobility of Molecular β-Copper Phthalocyanine Crystal
S. Pengmanayol, T. Osotchan, M. Suewattana, N. Ingadapa, J. Girdpun

086104 A Novel Large Moment Antiferromagnetic Order in $K_{0.8}Fe_{1.6}Se_2$ Superconductor
BAO Wei, HUANG Qing-Zhen, CHEN Gen-Fu, M. A. Green, WANG Du-Ming, HE Jun-Bao, QIU Yi-Ming

086201 Hydrogenic-Donor Impurity States in GaAs/$Al_xGa_{1-x}As$ Quantum Dots in the Presence of an Electric Field
PAN Jiang-Hong, LIU Li-Zhe, LIU Min

086401 FMAA-MS Investigation into $Ni_{68}Fe_{32}$ Nanoalloy with Sample Length Less than 30 mm
LI Ping-Yun, CAO Zhen-Hua, JIANG Zhong-Hao, MENG Xiang-Kang

086601 Stability of TiO_2 and Al_2O_3 Nanofluids
WANG Xian-Ju, LI Hai, LI Xin-Fang, WANG Zhou-Fei, LIN Fang

086602 Elimination of the Coherent Artifact in a Pump-Probe Experiment by Directly Detecting the Background-Free Diffraction Signal
LIU Hui, ZHANG Hang, SI Jin-Hai, YAN Li-He, CHEN Feng, HOU Xun

086801 Spectral Resolution Improvement of Mo/Si Multilayers
WU Wen-Juan, WANG Zhan-Shan, ZHU Jing-Tao, ZHANG Zhong, WANG Feng-Li, CHEN Ling-Yan, ZHOU Hong-Jun, HUO Tong-Lin

086802 Structural and Electronic Properties of Sulfur-Passivated InAs(001) (2×6) Surface
LI Deng-Feng , GUO Zhi-Cheng, LI Bo-Lin, DONG Hui-Ning, XIAO Hai-Yan

086803 Electrical, Structural and Interfacial Characterization of HfO_2 Films on Si Substrates
TAN Ting-Ting, LIU Zheng-Tang, LI Yan-Yan

CONDENSED MATTER: ELECTRONIC STRUCTURE, ELECTRICAL, MAGNETIC, AND OPTICAL PROPERTIES

087101 Dynamics of Exciton Diffusion in PVK:Phosphorescent Materials/Al Hetero-Structures
YANG Shao-Peng, HUANG Da, GE Da-Yong, LIU Bo-Ya, WANG Li-Shun, FU Guang-Sheng

087102 Growth and Properties of Blue and Amber Complex Light Emitting InGaN/GaN Multi-Quantum Wells
XIE Zi-Li, ZHANG Rong, LIU Bin, XIU Xiang-Qian, SU Hui, LI Yi, HUA Xue-Mei, ZHAO Hong, CHEN Peng, HAN Ping, SHI Yi, ZHENG You-Dou

087103 Electronic Properties of Boron Nanotubes under Uniaxial Strain: a DFT study
PAN Li-Jun, JIA Yu, SUN Qiang, HU Xing

087201 Current Transport in Copper Schottky Contacts to a-Plane/c-Plane n-Type $MoSe_2$
C. K. Sumesh, K. D. Patel, V. M. Pathak, R. Srivastav

087301 Leakage Current and Photovoltaic Properties in a $Bi_2Fe_4O_9$/Si Heterostructure
JIN Ke-Xin, LUO Bing-Cheng, ZHAO Sheng-Gui, WANG Jian-Yuan, CHEN Chang-Le

087302 Oscillations of Low-Field Magnetoresistivity of Two-Dimensional Electron Gases in $Al_{0.22}Ga_{0.78}N$/GaN Heterostructures in a Weak Localization Region
HAN Kui, TANG Ning, DUAN Jun-Xi, LU Fang-Chao, LIU Yu-Chi, SHEN Bo, ZHOU Wen-Zheng, LIN Tie, SUN Lei, YU Guo-Lin, CHU Jun-Hao

087303 Transformation from AA to AB-Stacked Bilayer Graphene on α-SiO_2 under an Electric Field
LIU Yan, AO Zhi-Min, WANG Tao, WANG Wen-Bo, SHENG Kuang, YU Bin

087304 Rectifying Characteristics and Transport Behavior in a Schottky Junction of $CaCu_3Ti_4O_{12}$ and Pt
CHEN Cong, NING Ting-Yin, WANG Can, ZHOU Yue-Liang,ZHANG Dong-Xiang, WANG Pei, MING Hai, YANG Guo-Zhen

087305 Influence of Fluorine on the Conductivity and Oxidation of Silicon Nanomembranes after Hydrofluoric Acid Treatment
ZHAO Xiang-Fu, HAN Ping, ZHANG Rong, ZHENG You-Dou

087306 Dipolar and Quadrupolar Modes of SiO_2/Au Nanoshell Enhanced Light Trapping in Thin Film Solar Cells
BAI Yi-Ming, WANG Jun, CHEN Nuo-Fu, YAO Jian-Xi, ZHANG Xing-Wang, YIN Zhi-Gang, ZHANG Han, HUANG Tian-Mao

087401 Influence of Magnetic Scattering and Interface Transparency on Superconductivity Based on a Ferromagnet/Superconductor Heterostructure
PENG Lin, LIU Yong-Sheng, CAI Chuan-Bing, ZHANG Jin-Cang

087402 Structural, Electronic and Optical Properties of $BiAl_xGa_{1-x}O_3$ (x= 0, 0.25, 0.5 and 0.75)
GONG Sai, WANG Yue-Hua, ZHAO Xin-Yin, ZHANG Min, ZHAO Na, DUAN Yi-Feng

087403 Fabrication of High-Quality Niobium Superconducting Tunnel Junctions
XU Qin-Yin, CAO Chun-Hai, LI Meng-Yue, JIANG Yi, ZHA Shi-Tong, KANG Lin, XU Wei-Wei, CHEN Jian, WU Pei-Heng

087501 Magnetic Performance of a Nanocomposite Permanent Material
LIU Min, HAN Guang-Bing, GAO Ru-Wei

087701 Piezoresponse Force Microscopy Imaging of Ferroelectric Domains in $Bi(Zn_{1/2}Ti_{1/2})O_3$-$Pb(Mg_{1/3}Nb_{2/3})O_3$-$PbTiO_3$ Piezoelectric Ceramics
LIU Li-Ming, ZENG Hua-Rong, CAO Zhen-Zhu, LENG Xue, ZHAO Kun-Yu, LI Guo-Rong, YIN Qing-Rui

087801 Femtosecond Pulse Propagation in a Symmetric Gap Surface Plasmon Polariton Waveguide
LU Zhi-Xin , YU Li, LIU Bing-Can, ZHANG Kai, SONG Gang

087802 Fast Modification of Microdischarge Emission Bands by Fracture of Sugar
Sergej Aman, Juergen Tomas, A. Streletskii

087803 Temperature-Induced Phase Transition of In_2O_3 from a Rhombohedral Structure to a Body-Centered Cubic Structure
YANG Lin-Hong, DONG Hong-Xing, SUN Zheng, SUN Liao-Xin, SHEN Xue-Chu, CHEN Zhang-Hai

087804 Optical Temperature Sensor Using Infrared-to-Visible-Frequency Upconversion in Er^{3+}/Yb^{3+}-Codoped Bi_3TiNbO_9 Ceramics
CHEN Heng-Zhi, YANG Bin, SUN Yan, ZHANG Ming-Fu, WANG Zhu, ZHANG Rui, ZHANG Zhi-Guo, CAO Wen-Wu

087805 Raman and Mid-IR Spectral Analysis of the Atacamite-Structure Hydroxyl/Deuteroxyl Nickel Chlorides $Ni_2(OH/D)_3Cl$
LIU Xiao-Dong, Hagihala Masato, ZHENG Xu-Guang, MENG Dong-Dong, GUO Qi-Xin

CROSS-DISCIPLINARY PHYSICS AND RELATED AREAS OF SCIENCE AND TECHNOLOGY

088101 Floating Zone Growth and Thermionic Emission Property of Single Crystal CeB_6
BAO Li-Hong, ZHANG Jiu-Xing, ZHOU Shen-Lin, ZHANG Ning, XU Hong

088301 Modeling of PZT Ferroelectric Ceramic Depolarization Driven by Shock Stress
LAN Chao-Hui, PENG Yu-Fei LONG Ji-Dong, WANG Qiang, WANG Wen-Dou

088501 Double-Teeth-Shaped Plasmonic Waveguide Electro-Optical Switches
ZHU Jia-Hu, HUANG Xu-Guang, MEI Xian

088502 Spin Filtering in a Nanowire Superlattice by Dresselhause Spin-Orbit Coupling
Samad Javidan

088701 Electronic Properties of the N_2C_4 Cluster of DNA
WANG Yong-Juan , CHENG Jie, YUE Xian-Fang

088702 Estimating RNA Loop Entropies Using a New Nucleobase Model and Sequential Monte Carlo Method
LIN Hui, ZHANG Jian

088703 Viscoelastic Characteristics of Fins, Muscle and Skin in Crucian Carp (Carassius Auratus) Described by the Fractional Zener Model
CHEN Ming, JIA Lai-Bing, YIN Xie-Zhen

GEOPHYSICS, ASTRONOMY, AND ASTROPHYSICS

089201 Non-Markovian and Non-Perturbative Entanglement Dynamics of Biomolecular Excitons
LIU Zhi-Qiang, LIANG Xian-Ting

089601 Magnetic Reconnection Under Solar Coronal Conditions with the 2.5D AMR Resistive MHD Model
ZHANG Shao-Hua, FENG Xue-Shang, WANG Yi, YANG Li-Ping

089701 PSR J1614-2230 May Include Hyperons
YU Zi, DING Wen-Bo, BAO Tmurbagan, LIU Ning-Ning

089702 Fermi γ-Ray Pulsars: Spectral and Generation Order Parameters
CAI Yan, A. Taani, WANG Wei, ZHAO Yong-Heng, ZHANG Cheng-Min

089801 Inflation and Singularity of a Bianchi Type-VII$_0$ Universe with a Dirac Field in the Einstein–Cartan Theory
HUANG Zeng-Guang, FANG Wei, LU Hui-Qing

089802 Locally Rotationally Symmetric Bianchi Type-II Magnetized String Cosmological Model with Bulk Viscous Fluid in General Relativity
Atul Tyagi, Keerti Sharma

089803 Bianchi Type-I Massive String Magnetized Barotropic Perfect Fluid Cosmological Model in the Bimetric Theory of Gravitation
N. P. Gaikwad, M. S. Borkar, S. S. Charjan